In-line near-infrared spectroscopy for the characterization of dispersion in polymer-clay nanocomposites

J.M. Barbas*, A.V. Machado, J.A. Covas

Institute for Polymers and Composites (IPC) and I3N, University of Minho, Campus of Azurém, 4800-058 Guimarães, Portugal

Keywords:

Near-infrared spectroscopy
Polymer nanocomposites
On-line monitoring
Melt-mixing

Abstract

In-line Near-Infrared spectroscopy (NIR) is used to monitor clay dispersion in the polymer matrix during the preparation of polymer nanocomposites by melt-mixing in a batch mixer. Based on chemometrics principles, various single parameter calibration models employing data obtained from widely used nanocomposite dispersion characterization techniques are developed and their quality tested. Given the generally unsatisfactory outcome, multi-parameter calibration models are then assessed, a 7-parameter model encompassing factors derived from oscillatory rheometry, FT-IR and thermomechanical data yielding good results. Since the validity of the model outside the material/equipment/ operating boundaries that were used to generate it was shown to be quite restricted, a second 7-parameter model is derived from a broader set of experimental data. Finally, the model is successfully applied to monitor in real time the evolution of clay dispersion with mixing time.

Introduction

Polymer nanocomposites based on layered silicate clays have found widespread practical application, as they possess good properties relative to the matrix even at low filler content

[1,2]. However, since performance is determined by the morphology and degree of clay dispersion attained during compounding and processing [1-4], it is important to carefully monitor and control these characteristics during those manufacturing stages. Therefore, the development of fast response and informative on-line techniques that are easy to operate, do not affect the existing material morphology at the monitoring location and that are sensitive even to minor changes in the material characteristics continues to be of great practical interest.

The authors have been using on-line oscillatory rheometry [5] for the characterization along the extruder of polymer-clay nanocomposites during compounding.

Although a good correlation seems to exist between the rheological response and the existing morphology or the degree of mixing, in some cases it may not be possible to discriminate between different dispersion levels [6,7]. Thus, the search for alternative on-line techniques remains relevant. In recent years, developments in sensors and fiber optics resulted in renewed interest in near-infrared spectroscopy (NIR) as an in-line technique for process monitoring/control purposes [8-10]. NIR spectroscopy is routinely utilized in several industrial polymer processes such as polymerization reactions, controlled degradation and chemical modification [8,11,12]. The use of NIR for inline monitoring of the preparation of polymer matrix nanocomposites is recent and limited. Moghaddam et al. [13] fixed a NIR probe to a compounding mini-extruder and correlated mixing temperature, particle size and viscosity changes with spectral differences. This was achieved by applying Principal Component scores, but no calibration model was defined. In turn, Witschnigg et al. [14] interfaced a NIR probe between a laboratory twin-screw extruder and the die and studied the effect of screw speed and geometry on the final properties of the

Table 1
Materials and main characteristics.

Material	Producer	Acronym	Grade	MFI/lamellar distance
Polypropylene	Lyondell Basell	PP	Moplen HP500N	12 g /10 min(230°C /2.16 kg)
Compatibilizer	Crompton	PP-g-MA	Polybond 3200	115 g /10 min(190°C /2.16 kg)
Montmorillonite clay	Southern Clay Products	C20A	Cloisite 20A	$d_{001} = 2.42$ nm

nanocomposites prepared. The authors developed single parameter calibration models, based on the Young's modulus, interlayer distance and drawing force, i.e., they focused on the clay reinforcement effects. However, the quality of some of the models seems insufficient to enable a quantitative analysis.

These efforts are encouraging in terms of exploring the possibility of correlating spectral differences of NIR data with clay dispersion levels. Due to the complexity of the spectra,

NIR should rely on adequate chemometrics to extract as much relevant information as possible from the data [8-10]. Chemometrics represents both NIR major advantage and limitation. Indeed, a single calibration model could eventually provide information on multiple chemical, physical and morphological characteristics, enabling NIR to replace several other characterization techniques. Conversely, an adequate chemometric analysis often requires extensive experimental characterization and data treatment, as well as the development of multiparameter calibration models [8-10,15,16].

This work uses NIR to monitor clay dispersion within a polymer matrix, both in terms of evolution with time and final level attained. A commercial set-up is used and a wide-ranging calibration model is developed to correlate NIR spectral data with nanocomposites morphology/ degree of mixing. To accomplish this, the usefulness of parameters derived from various well established characterization techniques is initially evaluated. A multiparameter calibration model is then put forward. The preparation of a polypropylene/polypropylene grafted with maleic anhydride/Montmorillonite clay system (PP/PP-gMA/C20A), using different PP-g-MA contents and operating conditions will be used as a case study. The compatibilizer content should impact on clay dispersion [22,29,31,32]. It has been reported that PP-g-MA contents of up to 15% wt. may induce high dispersion levels, a further increase in content having a negligible effect [22,31]. Similarly, different mixing speeds should bring about distinct degrees of dispersion [21-23,28].

Experimental

Materials and composites

The materials used in this work are listed in Table 1, together with their main characteristics. They include a commercial polypropylene (injection molding grade), a polypropylene grafted with maleic anhydride and Cloisite 20A, a natural montmorillonite clay modified with dimethyl dehydrogenated tallow quaternary ammonium salt (2 M 2 HT) in a concentration of 95meq/100 g of clay. Table 2 presents the compositions of one set of PP/PP-gMA/C20A nanocomposites containing the same amount of nanoclay (5 wt.%) and different PP-g-MA content (0 to 15wt. %), all prepared in a batch mixer (Haake Rheomix OS600 - Thermo Scientific Inc.) at 200°C and 50 rpm for 7 min , the ingredients being fed simultaneously. PP/PP-gMA/C20A with 90/5/5w/w/w was prepared using several rotor speeds (50, 100, 150 and 200 rpm).

In-line set-up

The in-line NIR system comprises three main components (Fig. 1): (i) a diffuse reflectance probe (Axiom Analytical Inc.) with a sapphire window having a diameter of 5.7 mm ; (ii) a Matrix ® F (Bruker Optics) spectrophotometer and (iii) the OPUS ® Quant2 (Bruker Optics) data acquisition and analysis software. The probe communicates with the spectrometer via a fiber optics cable and the spectrometer connects to the workstation by a LAN-type cable. A threaded hole with a Dynisco-type geometry was machined in the front plate of the mixing chamber to accommodate the NIR probe.

The NIR spectra were measured with a resolution of 8 cm^{-1} and accumulation of 4 scans, the acquisition time for each spectrum being less than 2 s . During the initial mixing stages, due to the melting of the matrix and the presence of large voids, the spectra were generally

very noisy and had very low absorbance. Consequently, for chemometric purposes acquisition started once the onset of equilibrium torque was reached (this typically occurred after 2 min of mixing), as the calibration models were developed for the final composites. Thus, it was possible to collect 150 spectra during each mixing cycle. Fig. 2(a) illustrates typical torque and temperature curves for PP and composites 95/0/5 and 85/15/5. Predictably, changes in composition cause variations in the maximum and equilibrium torque, as well as in the time to reach the latter, but only the maximum torque exhibits significant deviations. This may be due to the offsetting rheological effects of the PP-g-MA (decreasing the viscosity of the system) and of the clay (increasing the viscosity). Fig. 2(b) displays examples of the corresponding NIR spectra. The spectra measured soon after the material is fed ($t = 2$ s) are also included.

Characterization of the composites

Rotational rheometry (AR-G2, TA Instruments)

The linear viscoelastic response of the samples at 200°C was determined with oscillatory frequency sweeps from 0.1

Table 2
Compositions of the PP/PP-g-MA/C20A nanocomposites.

Material	Composition (wt.%)			
PP	95	90	85	80
PP-g-MA	0	5	10	15
C20A	5	5	5	5

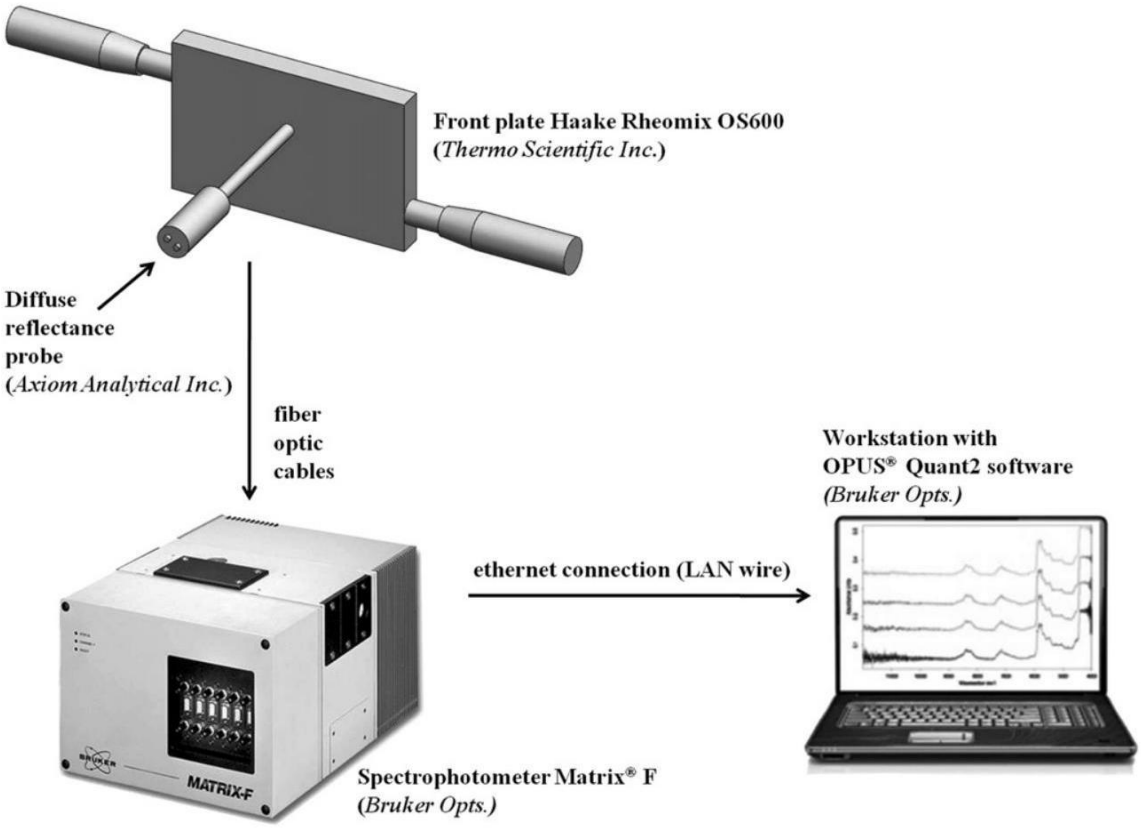

Fig. 1. In-line set-up.

to 100rad/s, using parallel plates with a diameter of 25 mm and a 1 mm gap, performed under constant strain (1% for the matrix and 0.5% for the composites). The disks were previously compression molded at 200°C and 20 tons. The complex viscosity vs. frequency curves were fitted to a modified Carreau-Yasuda model with yield stress, σ_0 [21-23]:

$$|\eta^*(\omega)| = \frac{\sigma_0}{\omega} + \eta_0[1 + \lambda\omega^a]^{(b-1)/a} \quad (1)$$

and to a power law (6-7):

$$|\eta^*(\omega)| = A\omega^b \quad (2)$$

where the adjustable parameters are the zero shear viscosity (η_0), the relaxation time (λ), the Yasuda parameter (a), the power law index (b) and the power law consistency (A). The Origin® Pro8 software was used for this purpose. The values of G′ (storage modulus) and G′′ (loss modulus) at low frequency were also determined.

Medium FT-IR (FTIR4100, Jasco)

The organoclay was analyzed with a KBr mortar. The nanocomposite samples were compression molded into thin films ($\pm 75\mu$ m thick) at 200 °C and analyzed in transmission mode, in a range between 4000 and 500 cm^{-1} using 10 scans and a resolution of 4 cm^{-1}. The wavelength region between 1300 and 750 cm^{-1} was fitted with the Pearson VII expression using the Origin [(8)] Pro8 software, with a 75% Gaussian shape (mu = 4) for the determination of the wavenumber shift for the 1050 cm^{-1} (Si – O in-

plane) and 1080 cm^{-1} (Si-O out-of-plane) peaks.
2.3.3 X-ray diffraction, XRD (AXS Nanostar-D8 Discover, Bruker)

The diffraction patterns were obtained using a diffractometer equipped with a CuKa generator ($\lambda = 1.5404Å$) at 40 kV and 40 mA , in a 2θ range from $0.08 - 10°$. The organoclay was analyzed directly ($\theta = 1.82°, d_{001} = 2.42$ nm), whereas the nanocomposite samples were previously compression molded into disks with a diameter of 20 mm and a thickness of 4 mm .

Tensile tests (Universal Tester 4505, Instron)

The testing procedure was in general accordance with ISO 527-3, using compression molded films ($\pm 250\mu$ m thick), a 1 kN load cell, a 50 mm initial gauge and a crosshead speed of 5 mm/min.

Development of the chemometric model

The measured NIR spectra are related to the clay dispersion state by means of a calibration model. To achieve this several aspects must be addressed, namely the selection of the parameters that most adequately describe the nanoclay dispersion (to be incorporated into the model), the determination of the minimum population size required to obtain a robust correlation and the definition of the best Validation/Calibration population size ratio, in order to minimize the monitoring time.

Chemometrics

Chemometrics is a step-by-step methodology aiming to develop a calibration model relating the NIR spectral data to the reference characterization parameters [8-10,16]. It

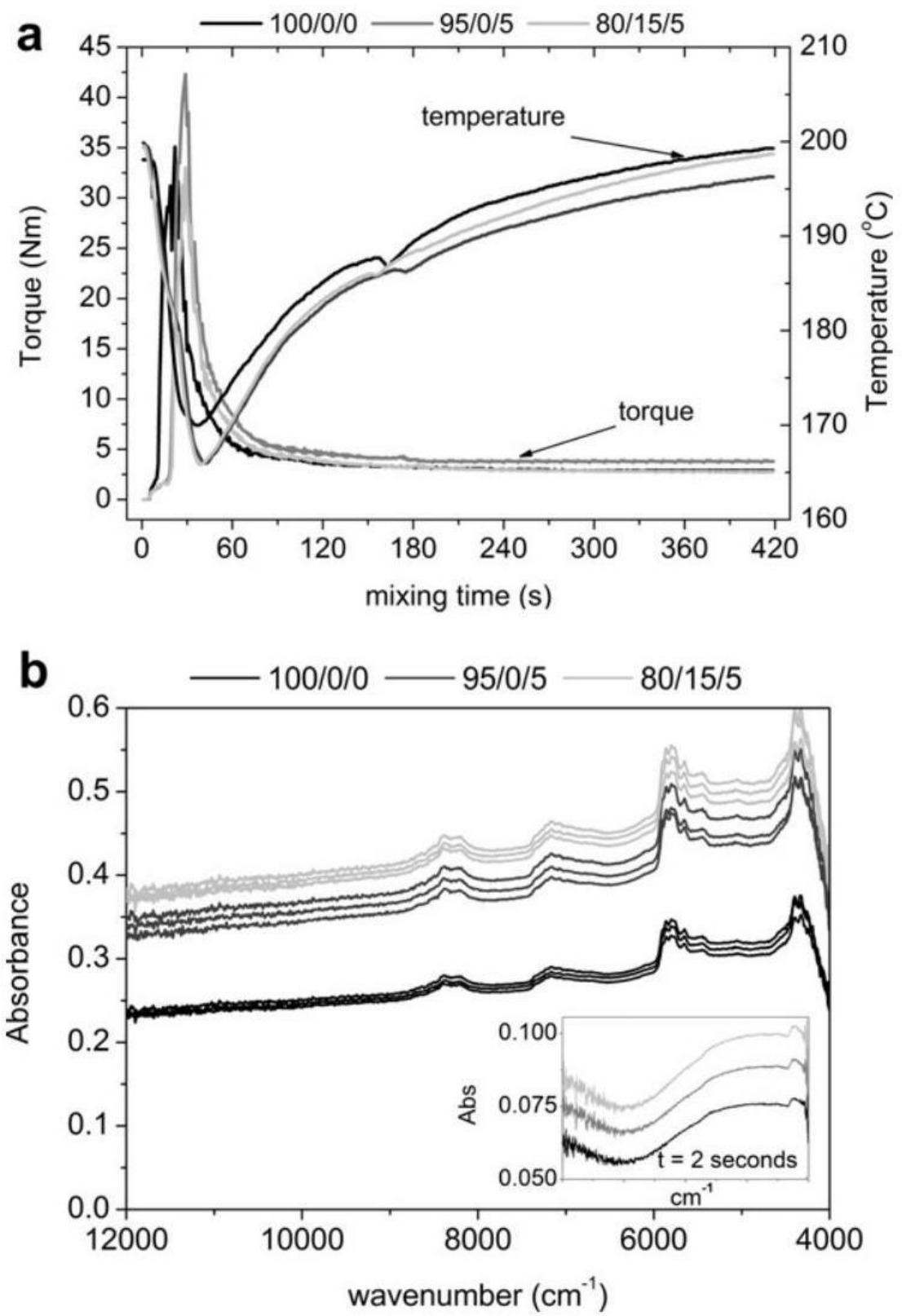

Fig. 2. (a) Typical batch mixer torque and temperature curves for samples 100/0/0, 95/0/5 and 80/15/5. (b) Examples of NIR spectra for the same materials.

involves the actual model development and its validation to guarantee effective predicting capabilities [10,16]. The multivariate calibration technique uses the entire spectral structures instead of a single spectral data point to provide broader information, and thus detect even minute differences in the sample spectra [9,16].

During model development, a pre-defined group of samples (commonly designated as "training samples") is used to compute the calibration curve, which directly yields the analyte property from the respective spectra. To ensure precision, the degree of correlation between the spectral and reference data should be high. For this purpose, a cross-validation step attests the quality of the adjustment of the data points to the calibration curve. More specifically, a certain number of the training samples are selected and the predicted property is compared with the reference values [10,16]. Finally, the calibration model can be used to predict the characteristics of unknown samples.

Quality of the model

A partial least squares (PLS) regression to the calibration data set was used, the model quality being assessed by the following parameters [9-11]:
i Error of prediction - the Root Mean Square Error is calculated for all samples:

$$RMSE = \sqrt{\frac{\sum_{i=1}^{n} \left(Y_{i_{\text{measured}}} - Y_{i_{\text{predicted}}}\right)^2}{n}} \tag{3}$$

where $Y_{measured}$ and $Y_{predicted}$ are the measured and predicted values, respectively. RMSE is usually labeled as Root Mean Square Error of Estimation (RMSEE) or as Root Mean Square Error of Prediction (RMSEP) when applied to model development or final independent validation, respectively. Both should be as low as possible.
ii. Coefficient of Determination (R^2) - it yields the percentage of variance present in the component values, which is reproduced in the subsequent prediction:

$$R^2 = \left[1 - \frac{\sum_{i=1}^{n} \left(Y_{i_{\text{predicted}}} - \overline{Y_{\text{predicted}}}\right)^2}{\sum_{i=1}^{n} \left(Y_{i_{\text{measured}}} - \overline{Y_{\text{measured}}}\right)^2}\right] \times 100 \tag{4}$$

where $\overline{Y_{predicted}}$ and $\overline{Y_{measured}}$ are the predicted and measured average values, respectively. Ideally, R^2 should be higher than 95%, but values above 90% are generally acceptable for qualitative studies. Low R^2 ($\ll 90\%$) frequently results from inappropriate reference parameters, insufficient precision of the reference data and/or presence of outliers in the calibration data set.
iii. Bias - is the systematic average deviation between the measured and predicted data sets, calculated by averaging all deviations in the data set:

$$\text{bias} = \frac{\sum_{i=1}^{n} \left(Y_{i_{\text{measured}}} - Y_{i_{\text{predicted}}}\right)^2}{n}$$

Bias should be as small as possible.
iv. Residual Prediction Deviation (RPD) - is the ratio between the standard deviation of the reference values and the bias-corrected mean error of the prediction (validation step):

$$RPD = \frac{\sqrt{\frac{1}{M-1} \times \sum_{i=1}^{n} \left(Y_{i_{\text{measured}}} - \overline{\overline{Y_{\text{measured}}}} \right)^2}}{\sqrt{\frac{1}{M-1} \times \sum_{i=1}^{n} \left(Y_{i_{\text{measured}}} - Y_{i_{\text{predicted}}} - \text{bias} \right)^2}} \quad (6)$$

where M is the size of the calibration set. Values above 5 are considered as adequate for quality control, whilst those over 8 indicate that the method is valid for analytical tasks.

Model parameters

In the present study, chemometrics will be employed to develop a calibration model able to predict the level of clay dispersion in a molten polymer matrix. This requires a proper characterization of the polymer-clay nanocomposite in order to find suitable reference parameters. Transmission electron microscopy (TEM) and X-ray diffraction (XRD) are probably the most commonly used techniques for this purpose [1,2,17-19]. TEM provides a direct view of clay dispersion, enabling the determination of agglomerates/particle size and number of stacks/platelets per area. However, TEM analyses only very small areas, requires time consuming sample preparation and tedious data treatment. XRD presents a clear region of interest at low 2θ angles, due to the typical clay Bragg's diffraction peak, from which the clay spacing and stacks height may be estimated. Nonetheless, XRD data may be misinterpreted due to orientation and crystallinity effects [1,2,17,18].

Several authors have successfully related the rheological response with the state of dispersion of clay nanocomposites [6,7,20-24]. For example, Lertwimolnun and Vergnes [21-23] used a modified Carreau-Yasuda model with yield stress (Eq. (1)) to describe the frequency dependence of the absolute complex viscosity, and successfully related this to the exfoliation level. Other studies used a power law expression to describe the complex viscosity and storage modulus behavior at low frequency, with the exponent correlating with the state of clay dispersion [6,7]. However, the same dependence was found both for high clay loading in a poorly dispersed composite and for good clay dispersion at lower clay concentration [6,7]. Also, the moduli values (G' and G'') may provide a good perception of dispersion, the increase of their values having been related to a finer dispersion [22], while the formation of a plateau at low frequencies has been attributed to the deformation and recovery of the dispersed particles [3,20,24].

Medium IR analysis (FT-IR) has also been utilized to characterize the morphology of polymer nanocomposites [25-27] based on the principle that the clay band can be decomposed into at least four peaks, three being related to the $Si-O$ in-plane vibrations (or bonds with basal oxygen) appearing at about 1120,1050 and 1020 cm^{-1}, respectively, and the fourth to the $Si-O^{-}$ out-of-plane vibration (with apical oxygen or hydroxyl group) appearing at about 1080 cm^{-1}. As the individual clay layers become more spaced, the peaks at 1050 cm^{-1} and 1080 cm^{-1} tend to shift. When the structure is ordered and intercalated, the peak at 1050 cm^{-1} will suffer a negative shift towards lower wavenumber, whilst for highly intercalated or partially exfoliated morphologies, the peak at 1080 cm^{-1} will shift to higher wavenumbers [26,27].

The mechanical properties (i.e., the practical material performance) should depend on the extent of dispersion, but the exact relation between them is much disputed [1,2,28-30]. The clay reinforcement effect is influenced by the adhesion between filler and matrix, the nanoparticle aspect ratio (individual layers, stacked layers or tactoids) and also by the clay

nucleating effect. For example, the role of the addition of a maleated compatibilizer [28,29] and of the preferential orientation of the clay platelets [30] on the mechanical performance has been investigated.

The above methods probe different length and time scales, thus possibly providing complementary sensitivities in terms of the degree of dispersion of a polymer/clay nanocomposite. Four of them will be taken as reference XRD, Rheology, FT-IR and tensile testing - as they are relatively simple to use and are readily available in most laboratories. Since, in principle, the final morphology of a polymer/clay system should result from the thermal and mechanical inputs during compounding/processing [21], it makes sense to include a thermomechanical index in this set. As a batch mixer is being used here, the maximum or the equilibrium torque per unit material were selected (the nominal values will be used, as the amount of composite in the mixing chamber was kept constant).

Results and discussion

Single parameter models

In the following, the parameters from each of the characterization techniques selected in Section 3.2 will be considered separately in terms of developing chemometric models, with the corresponding quality assessed by the measures also presented in Section 3.2. The experimental results obtained for the nanocomposites of Table 2 are listed in Table 3. Most parameters change monotonically with clay content, although some techniques seem to have difficulty in discriminating between the 89/10/5 and the 80/15/5 samples. Each calibration curve was determined with a partial least square regression on 150 spectra. Table 4 lists the respective quality factors. The R^2 and RPD values for the interlayer spacing (d_{001} from XRD), Young's modulus and maximum tensile stress are inferior to the

Table 3
Values of the parameters associated to the selected reference techniques.

		100/0/0	95/0/5	90/5/5	85/10/5	80/15/5
XRD	d_{001}(nm)	0.00	2.55	3.00	3.40	3.40
Rheology	G′(kPa)	0.073	0.118	0.186	1.061	1.003
	G″(kPa)	0.294	0.409	0.508	0.992	2.111
	σ_0(kPa)	0.000	0.037	0.129	1.356	2.250
	b	-0.194	-0.252	-0.240	-0.774	-1.000
FT-IR	1050 cm^{-1}	0.0	-3.1	-7.2	-8.4	-8.7
	1080 cm^{-1}	0.0	0.0	1.5	3.4	3.4
Tensile Testing	Young's Modulus (GPa)	1.200	1.180	1.135	1.124	1.103

	Maximum stress (MPa)	33.5	29.5	27.0	24.8	22.9
Torque	Maximum (Nm)	35.10	42.30	41.00	33.90	33.00
	Equilibrium (Nm)	2.98	3.80	3.47	3.23	2.89

Table 4
Quality factors of the individual calibration models and respective validation.

		XRD	Rheology				FT-IR		Tensile testing		Torque	
		d_{001} (nm)	G' (kPa)	G'' (kPa)	σ_0 (kPa)	b	1050 c	1080 c	E (GPa)	Stress (MPa)	Maximum (nm)	Equilibrium (nm)
Calibration	RMSEE	0.192	0.0068	0.0096	0.118	0.063	0.682	0.083	0.012	2.320	0.768	0.087
	R^2 (%)	68.8	97.8	98.2	99.1	98.5	96.3	99.1	89.1	62.7	93.1	91.6
	RPD	0.8	8.8	10.7	15.9	11.3	10.6	16.8	1.2	0.8	8.7	8.1
Validation	RMSEP	0.765	0.0999	0.112	0.154	0.101	0.236	0.102	0.234	3.96	1.982	0.108
	R^2 (%)	25.5	96.9	97.6	98.5	98.1	87.9	98.4	76.5	31.1	61.1	90.3
	bias	-2.86	0.16	0.12	0.10	-0.08	0.66	0.06	1.34	3.44	2.98	0.96

acceptable limits (90% for R^2 and 5 for RPD), i.e., it is not possible to build good calibration models using them. The validation step used 60 spectra per sample, i.e., a validation/calibration population ratio of 40%. As expected, interlayer spacing, Young's modulus and maximum tensile stress fail the validation step, as the predictive capability of the respective models is compromised by the low quality calibration results. As discussed above, even R^2 values above 90% do not necessarily guarantee a chemometric model with quantitative predictive power. As shown in Fig. 3 for the maximum torque and peak shift at 1050 cm^{-1}, the R^2 values of the calibration lines exceed 90% but the final validation fails because the model cannot resolve the spectral differences of the samples. In both cases the validation yields high global errors (RMSEP) and bias, as well as R^2 values below 90%. Several factors may influence these results, such as the limited sensitivity of the reference technique, the error associated with the reference results, insufficient data, influence of environmental conditions (temperature, humidity) and sample preparation. The remaining parameters, namely rheology data, peak shift at 1080 cm^{-1} and equilibrium torque provide robust models, for which the quality of the calibration was supported by the validation results.

Overall, these results express the ineffectiveness of single parameters such as d_{001}, Young's modulus and maximum tensile stress to describe the global state of clay dispersion in the polymer matrix, which confirms the possibility of secondary effects influencing the results, as discussed in Section 3.3.

Population size

Sampling size and ratio between the validation and calibration populations could influence the quality of the chemometric models. In order to investigate this, the single parameter models were recalculated for different population sizes. The 150 spectra registered initially were divided in two groups, one containing 100 spectra to be used for calibration and the other with 50 spectra to be used for validation. Assignment to the groups was done randomly. Subsequently, sub-groups formed from these rendered different calibration population sizes and validation/calibration population ratios. As far as calibration is concerned, the size of the population was found to have little influence on the chemometric values. For example, the R^2 of d_{001} ranges between 69.9% and 68.8% when the population size increases from 25 to 100, maintaining the value of 68.8% for a population of 150 . Similar conclusions could be reached for the remaining parameters. Table 5 presents the R^2 and RMSEP values for the validation for several validation/calibration population ratios (ranging from 5 to 60%). The Validation/Calibration population ratio does not affect the quality of the models. The exceptions are the torque parameters, particularly the maximum torque, for which the decrease in the population ratio from 60% to 5% results in R^2 values exceeding the acceptable 90%.

Overall, these data confirm the results presented in Section 4.1 and show that the development of a reliable chemometric model does not rely on the sampling size of the calibration, but rather on the effectiveness of the parameters used.

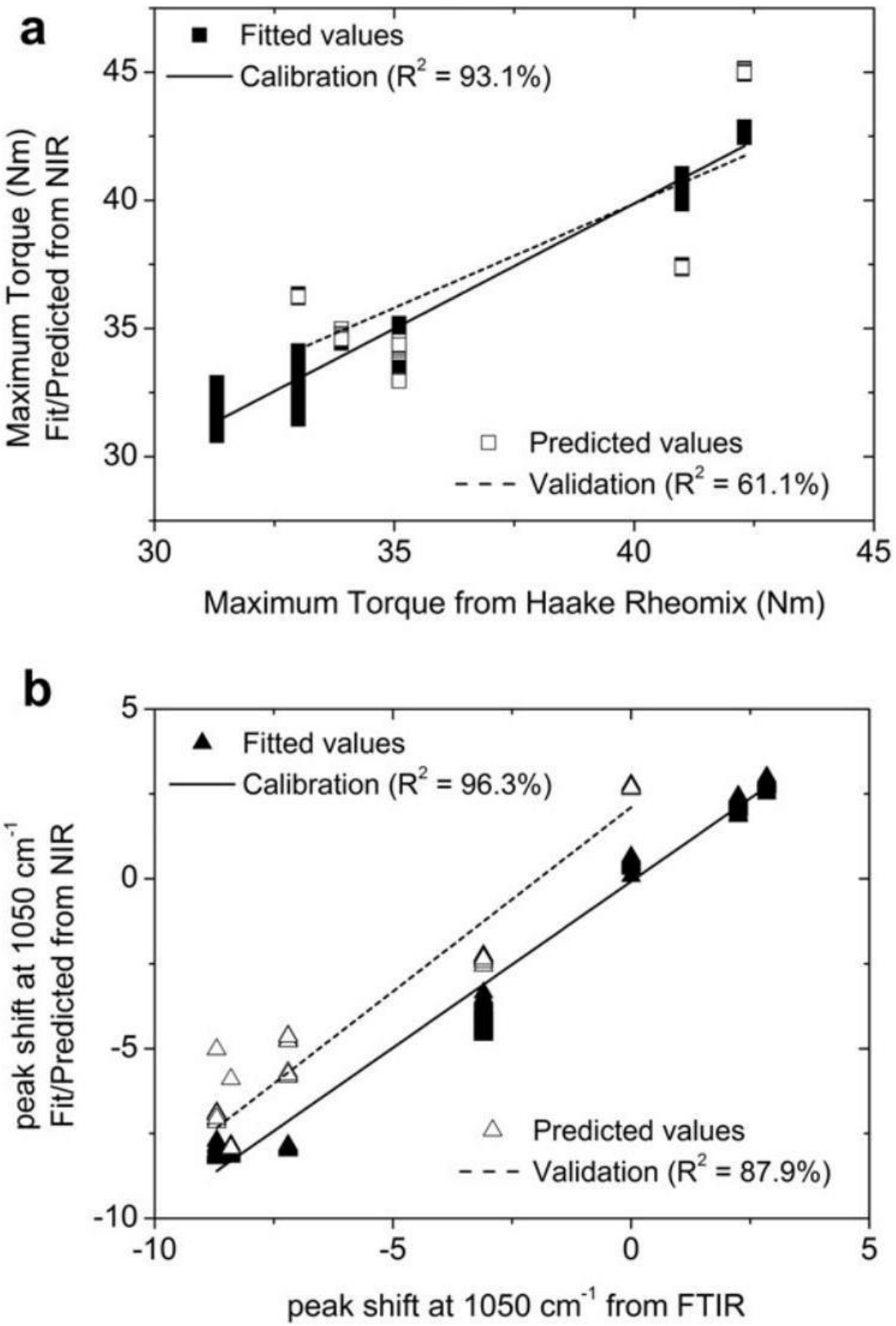
a
Fitted values
Calibration (R^2 = 93.1%)
Predicted values
Validation (R^2 = 61.1%)
Maximum Torque (Nm)
Fit/Predicted from NIR
Maximum Torque from Haake Rheomix (Nm)
45
40
35
30
30
35
40
45
b
Fitted values
Calibration (R^2 = 96.3%)
Predicted values
Validation (R^2 = 87.9%)
peak shift at 1050 cm^{-1}
Fit/Predicted from NIR
peak shift at 1050 cm^{-1} from FTIR
5
0
-5
-10
-10
-5
0
5

Fig. 3. Individual calibration models and their validation: (a) Maximum torque; (b) peak shift at 1050 cm^{-1}.

Table 5
Validation of the chemometric models using different validation/calibration population ratios.

Validation/Calibration (%)		5	15	25	60
XRD	d_{001}(nm)	60.3/0.19	60.1/0.19	59.6/0.19	59.0/0.19
	G′(kPa)	95.7/0.11	95.2/0.10	94.4/0.11	93.1/0.12
Rheology	G′′(kPa)	96.9/0.17	96.4/0.14	95.6/0.17	95.5/0.20
	σ_0(kPa)	97.5/0.09	97.4/0.10	96.7/0.09	95.8/0.11
	b	96.4/0.14	95.8/0.14	95.1/0.14	94.3/0.19
FT-IR	1050 cm^{-1}	94.1/0.07	93.8/0.06	93.5/0.06	92.2/0.06
	1080 cm^{-1}	96.4/0.12	95.9/0.11	95.6/0.13	94.9/0.13
Tensile Testing	Young's Mod. (GPa)	86.1/0.10	86.5/0.10	86.0/0.10	85.4/0.10
	Maximum stress (MPa)	59.0/2.34	59.4/2.32	59.2/2.37	58.6/2.42
Torque	Maximum (Nm)	91.7/0.91	90.7/0.70	88.9/0.77	88.9/0.98
	Equilibrium (Nm)	90.5/0.11	89.7/0.11	89.3/0.13	88.6/0.15

Multi-parameter models

The ineptitude of single model parameters based on d_{001}, Young's modulus and maximum tensile stress to describe the global state of clay dispersion in the polymer matrix having been demonstrated, the suitability of multiparameter models was explored. In this case, each parameter was normalized as:

$$\text{Normalized Value (\%)} = \frac{(\text{Value} - \text{minimum})}{(\text{maximum} - \text{minimum})} \times 100$$

i.e., a score of 0% matches the polymer matrix, while 100% refers to the best dispersed nanocomposite. In turn, each model considered the average of the relevant normalized values. Table 6 presents the calibration and validation quality factors of the various models tested combining from 2 to 11 parameters. A model joining more than one parameter, even if extracted from a single characterization technique, is taken here as multiparameter.

For a population of 150 spectra per sample and a validation/calibration population ratio of 15%, the torque parameters, merging rheology and XRD, and grouping rheology, FT-IR and tensile testing resulted in calibration lines with high coefficients of determination

but poor validation outcomes. Combining the 11 parameters yields a chemometric model with very low calibration and validation R^2 values (51.7% and 38.5%, respectively).

Conversely, using the FT-IR parameters, the (four) rheology parameters and the combination of both techniques yielded excellent calibration lines, with R^2 values above 98% and very good validation performance. Fig. 4 shows the best result, which was obtained with a 7 parameter model encompassing the maximum torque, storage (G') and loss (G'') moduli, melt yield stress (σ_0), power law index (b) and peak shifts at 1050 and 1080 cm^{-1}. The calibration curve has a global error (RMSEE) of 0.85 , a residual prediction deviation (RPD) of 27.8 , and a R^2 value of 99.8%. As for the validation, the results were also very good, with R^2 equal to 99.5%, a global error of 1.01 and a bias of 0.641 .

These results could be foreseen taking into consideration those presented in Section 4.1. If the parameters derived from XRD and tensile testing do not yield good quality single parameter models, using them in multiparameter arrangements will compromise the quality of the final model. The same reasoning should be applicable to the higher quality models, which combine parameters that previously rendered good single parameter models.

The results above exhibit a number of interesting features:

- Despite the supporting rationality and the ease of obtaining their parameter values, it seems that models attempting to adopt global energy inputs to the system upon mixing have difficulty in correlating them strongly with the resulting dispersion. Other authors have reported similar difficulties [21,29,31,32].
- Parameters from well established characterization techniques such as rheology (oscillatory rheometry) and FT-IR, but not XRD as seen above, can provide very good chemometric models and so does their combination.
- As expected, the combination of favorable techniques, such as rheology and FT-IR, with others yielding weaker chemometric models (e.g., XRD or tensile data) compromises the usefulness of the exercise; this is particularly noticeable in the 11 parameter model, which presented the worst quality.
- Conversely, developing multi-parameter models that incorporate sufficiently performing building blocks generates adequate chemometric models, such as the 7-parameter tested.

Table 6
Calibration and validation results for the multi-parameter models.

Multi-parameter model	Calibration			Validation		
	R^2 (%)	RMSEE	RPD	R^2 (%)	RMSEP	Bias
Torque	95.6	1.52	9.0	89.7	1.99	-3.09
FT-IR	98.5	0.23	12.8	98.1	0.47	0.81
Rheology	98.8	0.65	13.1	96.9	1.12	0.87

Rheology and XRD	94.0	2.09	8.0	90.1	4.15	1.14
Rheology and FT-IR	98.6	0.76	14.5	97.7	0.97	-0.75
Maximum torque, Rheology and FT-IR	99.8	0.85	27.8	99.5	1.01	0.64
Rheology, FT-IR and Tensile testing	90.4	1.67	8.1	88.2	2.14	1.08
All	51.7	10.1	1.8	38.5	22.3	-15.7

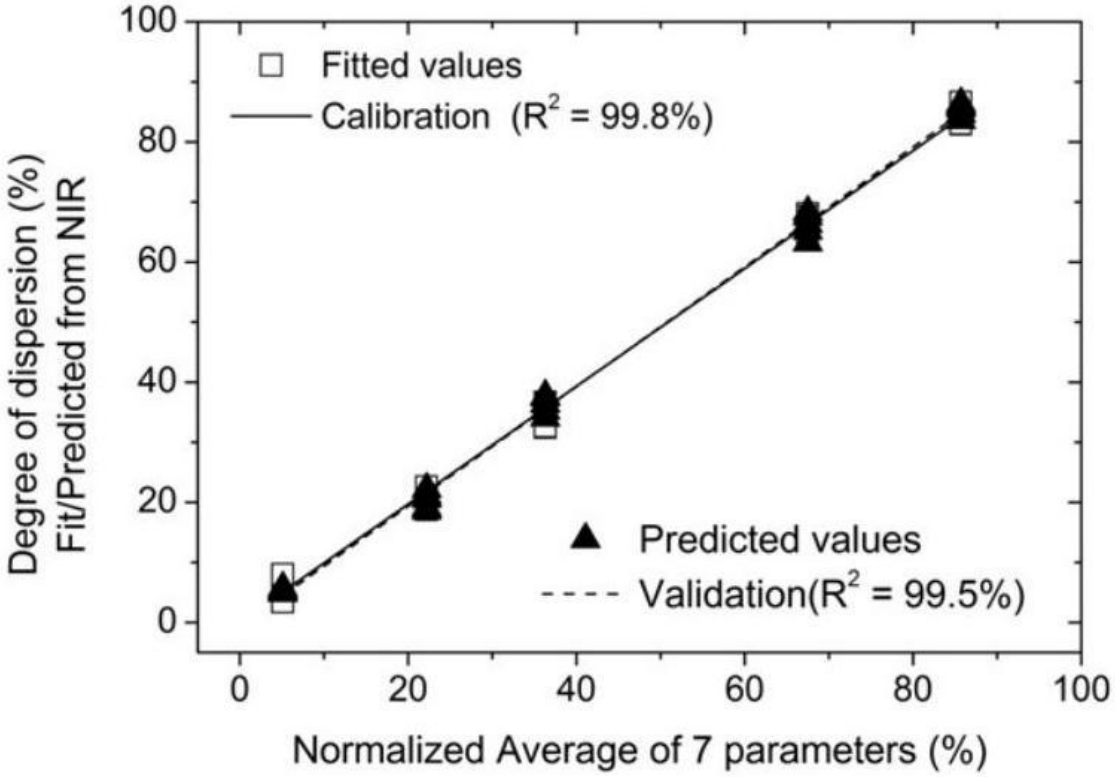

Fig. 4. Chemometric model using the normalized average of maximum torque, rheology and FT-IR.

Validity limitations

The 7-parameter model discussed above and developed from samples prepared with different PP-g-MA content was employed to characterize the degree of dispersion of nanocomposites prepared with different rotor speeds. In Table 7, the predictions show good agreement with the measured values for 50 rpm , but the differences for the samples prepared at the remaining speeds range between 14 and 32%. This is generally translated by the high RMSEP and bias. The good outcome for 50 rpm is explained by the fact that this condition was used in the two sets of nanocomposite samples (Section 2.1). Thus, the 7-parameter model developed based on the effect of the PP-g-MA content is not suitable to analyze samples prepared under different operating conditions, i.e., NIR-based models

should not be applicable outside the material/equipment/ operating boundaries that were used to generate them. Although not shown here, the application of the 7parameter model based on data from nanocomposites prepared under different rotor speeds would face identical limitations in characterizing the dispersion of nanocomposites with varying degrees of compatibilizer.

Given the above, it makes sense to use the data from the two sets of experiments (exploring the effects of PP-g-MA content and of rotor speed) to generate a new 7parameter chemometric model. The normalized average values of all samples were recalculated, as the absolute minimum and maximum values of each parameter are now altered. Table 8 summarizes the quality factors. The new global model exhibits a high quality standard, with

Table 7
Predicted final dispersion level of nanocomposites prepared using different rotor speeds.

	50 rpm	100 rpm	150 rpm	200 rpm
Measured (±error)	27.5(±3.3)	34.5(±4.7)	52.4(±6.1)	79.2(±9.7)
Predicted (± error)				
RMSEP	22.4			
Bias	20.6			

Table 8
Global 7-parameter model: calibration and validation quality factors.

Calibration			Validation		
R^2(%)	RMSEE	RPD	R^2(%)	RMSEP	Bias
99.5	1.52	14.2	99.1	2.03	-0.013

a calibration curve with R^2 above 99%, a low global error and a high RPD, and validation with a R^2 value above 90%, low global error and a bias approaching zero. For example, when using the initial 7 - parameter model to predict the dispersion level of the samples prepared with different PP-g-MA content (Fig. 4), the differences between measurements and forecasts ranged in the interval 1.3% to 3.9%. The new global 7 - parameter produces discrepancies in the range 0.3 – 1.5%.

Real-time prediction

The predictive ability of the global model in real-time NIR measurements will be used to monitor the evolution of dispersion upon mixing. Since the global model was developed taking in two variables - PP-g-MA content and rotor speed - these effects were studied independently. Thus, a new composite containing 7.5%wt. of PP-g-MA (87.5/7.5/5) was prepared at a rotor speed of 50 rpm (the reference rotor speed). In turn, the 90/5/5w/w/w composite (the reference composite) was prepared at 125 and 175 rpm . Spectra were

collected every 2 s , Fig. 5 showing data for the 87.5/7.5/5w/w/w nanocomposite. Fig. 6 presents the evolution in time of torque and the predicted dispersion level for the two case studies.

The initial spectrum (at 0 s) is close to zero. As mixing evolves, both the baseline and the signal intensity increase. As seen in the torque curve, melting starts at around 1020 s of mixing. The increase in torque is due to the conversion of a granular flow into that of a melt suspension with high solids content. Even in these initial moments, although the NIR signal is weak, the fundamental peaks are already visible, and clay dispersion is predicted to be initiated. The torque reaches its maximum at about 30 s and decreases thereafter as melting progresses. Melting is probably completed at around 90-120 s, but it is only after

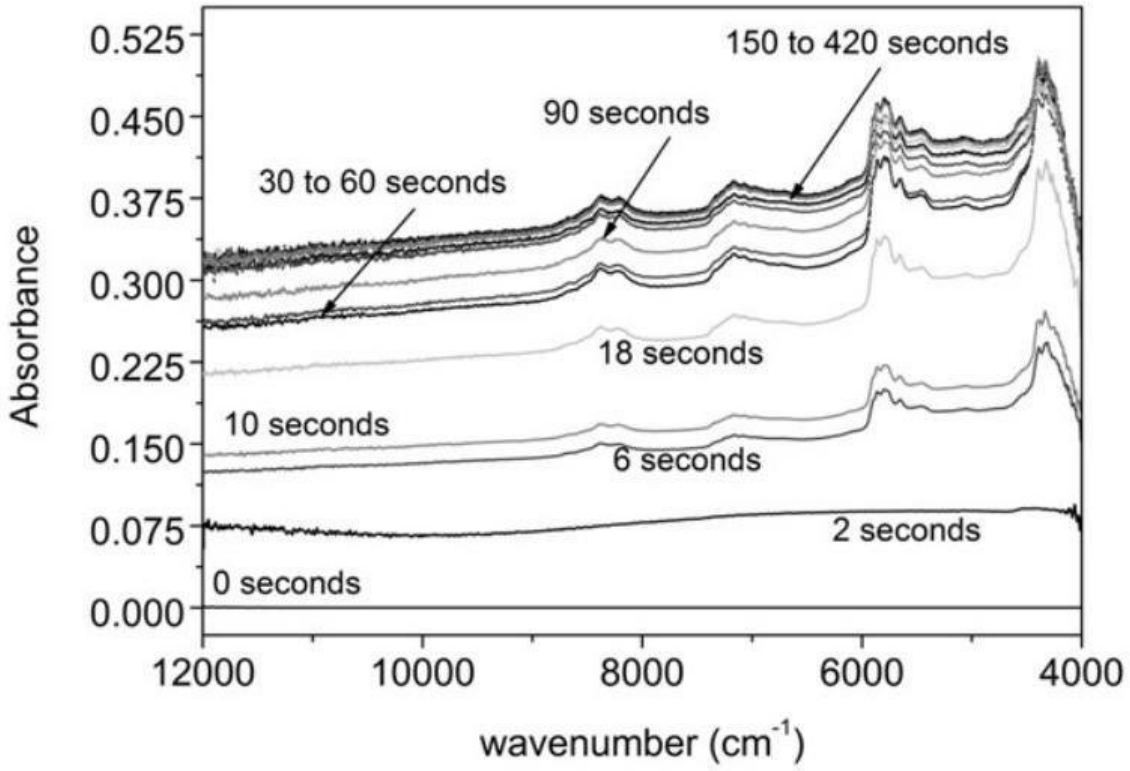

Fig. 5. Spectra measured during mixing for 87.5/7.5/5w/w/w.

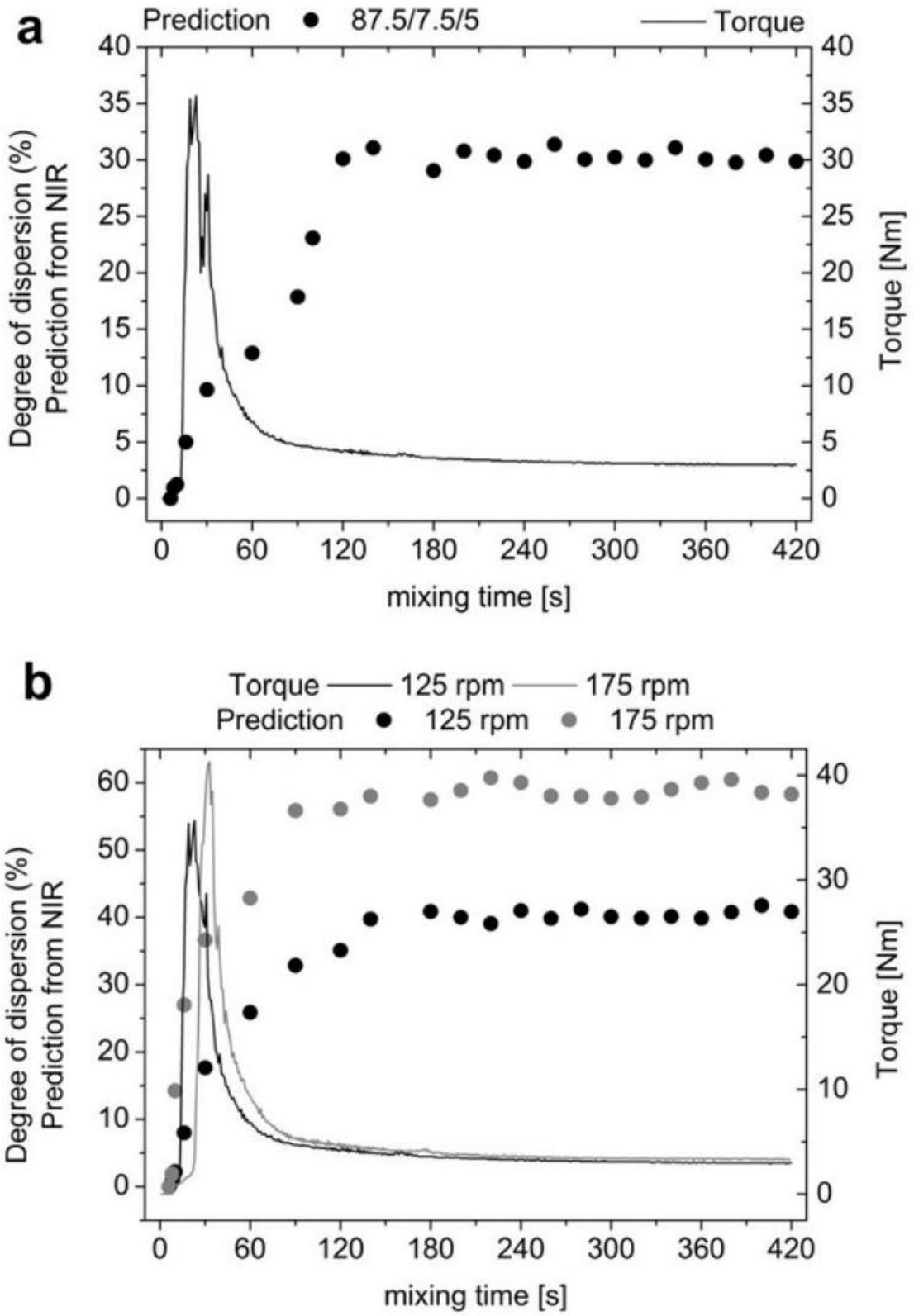

Fig. 6. Time evolution of torque and (predicted) dispersion: (a) 87.5/7.5/5 at 50 rpm (b) 90/5/5 at 125 and 175 rpm .

mixing for 180 s that a torque plateau is reached, which most likely corresponds to little further changes in dispersion. In fact, it has been repeatedly reported for several systems melt mixed in batch mixers or twin-screw extruders that most of the dispersive mixing takes place upon melting, when the thermomechanical stresses are higher, little evolution being detected thereafter [33,34]. Differences in the NIR spectra are also higher in the same interval, whereas between 180 to 420 s the spectra are nearly superimposed. Thus, the rate of dispersion is predicted to be higher from 60 to 150 s and a plateau is foreseen beyond 180 s .

The final dispersion level (after 180 s) predicted by NIR for the sample with 7.5% wt of PP-g-MA is roughly 30%, which connects well with the normalized average values of the samples with 5% and 10% wt. of PP-g-MA, 26.3% and 36.9%, respectively. It is also in agreement with reports relating the improvement of clay dispersion in polyolefin matrices with the increase in compatibilizer content [22,29,31,32]. In the case of the 90/5/5w/w/w nanocomposite, the final dispersion level is predicted to increase with rotor speed (approximately 39% and 59% at 125 rpm and 175 rpm , respectively). Again, these values are in line with the normalized averages (23.5%, 49.6%, 77.2% for 100 , 150 and 200 rpm , respectively) and with reports showing an increase in dispersion with increasing rotor speed [21-23,28].

Conclusions

The viability and effectiveness of using NIR for the inline monitoring of clay dispersion during the preparation of clay nanocomposites by melt-mixing is demonstrated. Chemometrics can support the development of calibration models with good quality calibration and validation measures, but two requirements must be fulfilled. First, it is essential that models are built with parameters from dispersion characterization techniques that are really able to discriminate between distinct dispersion levels. In this respect, the implementation of single parameter calibration models from XRD, rheology, FT-IR, tensile testing or torque data was globally unsuccessful. Multi-parameter models showed greater potential, particularly when incorporating sufficiently performing individual building blocks. Specifically, a 7-parameter model incorporating parameters from oscillatory rheometry (G', G'', σ_0, b), FT-IR (wavenumber shift of the peaks at 1050 and 1080 cm^{-1}) and thermomechanical data from the mixing equipment (maximum torque) yielded good results. Secondly, it was proven that the validity of the calibration model outside the material/equipment/operating boundaries that were used to create it is very limited. Therefore, it is important to use the broadest possible set of data. In the present case, the same 7-parameter model now based on results from nanocomposites produced at different rotor speeds and having different compatibilizer levels exhibited very good quality features. When applying this same calibration model to the real time monitoring of the evolution of dispersion upon mixing of nanocomposites under new operating conditions or of nanocomposites containing new levels of compatibilizer, not only distinct results were obtained, but they matched well the forecasted values.

Finally, an investigation of the effect of population size on the quality of the calibration model showed that when setting the Validation/Calibration population ratio at 15% there is no need to use an extensive sampling size.

References

[1] M. Alexandre, P. Dubois, Polymer-layered silicate nanocomposites: preparation, properties and uses of a new class of materials, Materials Science and Engineering 28 (2000) 1-63.
[2] D.R. Paul, L.M. Robeson, Polymer nanotechnology: nanocomposites, Polymer 49 (2008) 3187-3204.
[3] S.S. Ray, M. Okamoto, Polymer/layered silicate nanocomposites: a review from preparation to processing, Progress in Polymer Science 28 (2003) 1539-1641.
[4] S. Pavlidou, C.D. Papaspyrides, A review on polymer-layered silicate nanocomposites, Progress in Polymer Science 33 (2008) 1119-1198.
[5] S. Mould, J.M. Barbas, A.V. Machado, J.M. Nóbrega, J.A. Covas, Measuring the rheological properties of polymer melts with on-line rotational rheometry, Polymer Testing 30 (2011) 602-610.
[6] A. Durmus, A. Kasgoz, C.W. Macosko, Linear low density polyethylene (LLDPE)/clay nanocomposites. Part I: structural characterization and quantifying clay dispersion by melt rheology, Polymer 48 (2007) 4492-4502.
[7] A. Vermogen, K. Masenelli-Varlot, R. Séguéla, J. Duchet-Rumeau, S. Boucard, P. Prele, Evaluation of the structure and dispersion in polymer-layered silicate nanocomposites, Macromolecules 38 (2005) 9661-9669.
[8] M. Blanco, I. Villarroya, NIR spectroscopy: a rapid-response analytical tool, Trends in Analytical Chemistry 21 (2002) 240-249.
[9] D.A. Burns, E.W. Ciurczak (Eds.), Handbook of Near-Infrared Analysis, CRC Press, 2008.
[10] H.W. Siesler, Y. Ozaki, S. Kawata, H.M. Heise, Near-Infrared Spectroscopy: Principles, Instruments, Applications, Willey-VCH, 2002.
[11] A.F. Santos, E.L. Lima, J.C. Pinto, In-line evaluation of average particle size in styrene suspension polymerizations using near-infrared spectroscopy, Journal of Applied Polymer Science 70 (1998) 17371745.
[12] S.E. Barnes, M.G. Sibley, H.G.M. Edwards, P.D. Coates, Process monitoring of polymer melts using in-line spectroscopy, Transactions of the Institute of Measurement and Control 29 (2007) 453-465.
[13] L. Moghaddam, D.J. Martin, P.J. Halley, P.M. Fredericks, Vibrational spectroscopic studies of laboratory scale polymer melt processing: application to a thermoplastic polyurethane nanocomposite, Vibrational Spectroscopy 51 (2009) 86-92.
[14] A. Witschnigg, S. Laske, M. Kracalik, M. Feuchter, G. Pinter, G. Maier, W. Märzinger, M. Haberkorn, G.R. Langecker, C. Holzer, In-line characterization of polypropylene nanocomposites using FT-NIR, Journal of Applied Polymer Science 117 (2010) 3047-3053.
[15] J. Workman Jr., L. Weyer, Practical Guide to Interpretive NearInfrared Spectroscopy, CRC Press, 2007.
[16] M.J. Adams, Chemometrics in Analytical Spectroscopy, The Royal Society of Chemistry, 1995.
[17] A.B. Morgan, J.W. Gilman, Characterization of polymer-layered nanocomposites by transmission electron microscopy and x-ray diffraction: a comparative study, Journal of Applied Polymer Science 87 (2003) 1329-1338.
[18] B.N. Jang, D. Wang, C.A. Wilkie, Relationship between the solubility parameter of polymers and the clay dispersion in polymer/clay nanocomposites and the role of the surfactant, Macromolecules 38 (2005) 6533-6543.
[19] J. Bandyopadhyay, S.S. Ray, The quantitative analysis of nano-clay dispersion in polymer nanocomposites by small angle X-ray scattering combined with electron microscopy, Polymer 51 (2010) 1437-1449.
[20] M.J. Solomon, A.S. Almusallam, K.F. Seefeldt, A. Somwangthanaroj, P. Varadan,

Rheology of polypropylene/clay hybrid materials, Macromolecules 34 (2001) 1864-1872.
[21] W. Lertwimolnun, B. Vergnes, Influence of screw profile and extrusion conditions on the microstructure of polypropylene/organoclay nanocomposites, Polymer Engineering and Science 47 (2007) 2100-2109.
[22] W. Lertwimolnun, B. Vergnes, Influence of compatibilizer and processing conditions on the dispersion of nanoclay in a polymer matrix, Polymer 46 (2005) 3462-3471.
[23] W. Lertwimolnun, B. Vergnes, Effect of processing conditions on the formation of polypropylene/organoclay nanocomposites in a twin-screw extruder, Polymer Engineering and Science 46 (2006) 314-323.
[24] P. Cassagnau, Melt-rheology of organoclay and fumed silica nanocomposites, Polymer 49 (2008) 2183-2196.
[25] L. Yan, C.B. Roth, P.F. Low, Changes in the Si-O vibrations of smectite layers accompanying the sorption of interlayer water, Langmuir 12 (1996) 4421-4429.
[26] L.S. Loo, K.K. Gleason, Fourier transform infrared investigation of the deformation behavior of montmorillonite in nylon-6/nanoclay nanocomposite, Macromolecules 36 (2003) 2587-2590.
[27] K.C. Cole, Use of infrared spectroscopy to characterize clay intercalation and exfoliation in polymer nanocomposites, Macromolecules 41 (2008) 834-843.
[28] M. Modesti, A. Lorenzetti, D. Bon, S. Besco, Effect of processing conditions on morphology and mechanical properties of compatibilized polypropylene nanocomposites, Polymer 46 (2005) 1023710245.
[29] M.W. Spencer, L. Cui, Y. Yoo, D.R. Paul, Morphology and properties of nanocomposites based on HDPE/HDPE-g-MA blends, Polymer 51 (2010) 1056-1070.
[30] M. Bousmina, Study of intercalation and exfoliation processes in polymer nanocomposites, Macromolecules 39 (2006) 4259-4263.
[31] D.H. Kim, P.D. Fasulo, W.R. Rodgers, D.R. Paul, Structure and properties of polypropylene-based nanocomposites: effect of PP-g-MA to organoclay ratio, Polymer 48 (2007) 5308-5323.
[32] K. Chrissopoulou, S.H. Anastasiadis, Polyolefin/layered silicate nanocomposites with functional compatibilizers, European Polymer Journal 47 (2011) 600-613.
[33] J.A. Covas, O.S. Carneiro, J.M. Maia, S.A. Filipe, A.V. Machado, Evolution fo chemistry, morphology and rheology of various polymer systems along a twin-screw extruder, The Canadian Journal of Chemical Engineering 80 (2002) 1065-1074.
[34] J.K. Lee, C.D. Han, Evolution of polymer blend morphology during compounding in an internal mixer, Polymer 40 (1999) 62776296.

E-mail address: joana.barbas@dep.uminho.pt (J.M. Barbas).